

1 Article

# 2 Customizable vector acceleration in extreme-edge 3 computing: a RISC-V software/hardware architecture 4 study on VGG-16 implementation

5 Stefano Sordillo<sup>1</sup>, Abdallah Cheikh<sup>1</sup>, Antonio Mastrandrea<sup>1</sup>, Francesco Menichelli<sup>1</sup>, Mauro  
6 Olivieri<sup>1,\*</sup>

7 <sup>1</sup> DIET, Sapienza University of Rome

8 \* Correspondence: mauro.olivieri@uniroma1.it

9 Received: date; Accepted: date; Published: date

10 **Abstract:** Computing in the cloud-edge continuum, as opposed to cloud computing, relies on high  
11 performance processing on the extreme edge of the IoT hierarchy. Hardware acceleration is a  
12 mandatory solution to achieve the performance requirements, yet it can be tightly tied to particular  
13 computation kernels, even within the same application. Vector-oriented hardware acceleration has  
14 gained renewed interest to support AI applications like convolutional networks or classification  
15 algorithms. We present a comprehensive investigation of the performance and power efficiency  
16 achievable by configurable vector acceleration subsystems, obtaining evidence of both the high  
17 potential of the proposed microarchitecture and the advantage of hardware customization in total  
18 transparency to the software program.

19 **Keywords:** edge-computing, processors, hardware acceleration

20

## 21 1. Introduction

22 The cloud-edge continuum computing paradigm relies on the possibility of local processing in  
23 the edge of the IoT whenever it is convenient for reasons of energy efficiency, reliability, or data  
24 security. As a consequence, there is a gradual shift of artificial intelligence (AI) algorithm execution  
25 from the cloud down low power embedded IoT devices on the edge, to be used in real-time for  
26 example to take voice commands or extract image features, for biometric, security, or filtering  
27 purposes [5].

28 The resultant demand for very high processing speed on extreme edge computing devices turns  
29 into unprecedented design challenges, especially because of the usually limited energy budget.  
30 Therefore, the implementation of hardware acceleration on edge devices in the IoT hierarchy has  
31 become a major trend to reach the speed and energy efficiency requirements.

32 Vector computing acceleration was a major stream in high performance computing systems for  
33 decades and is gaining renewed interest in recent development in the supercomputing sector [22].  
34 Yet, it is easy to note that the vector computing paradigm can also be applied to AI computing kernels  
35 that are run in embedded IoT devices on the edge. Nonetheless, the limited hardware budget usually  
36 available in edge devices makes it interesting to explore the possibility of configurable acceleration  
37 sub-systems to optimally exploit the available hardware resources according to the specific  
38 computation kernels being run during the application execution.

39 We implemented such exploration addressing the execution of the VGG-16 deep convolutional  
40 neural network inference, widely known for its image recognition performance as well as for the high  
41 computing power and storage demand. The VGG-16 execution is composed of consecutive layers  
42 having different computational characteristics. Therefore, it well represents a stress-test of the  
43 hardware micro-architecture with a time-variant workload profile. Our target micro-architecture is

44 an open-source RISC-V [3] processor core supporting multi-threaded execution and featuring a  
45 highly customizable vector acceleration subsystem [23].

46 The contributions of this work to the reader interested in advanced embedded system design for  
47 IoT extreme-edge computing, are manifold:

- 48 • we report the quantitative evidence of the trade-offs in vector co-processor design and  
49 configuration targeting simple edge-computing soft-cores;
- 50 • we present details on the small custom RISC-V compliant instruction extension  
51 sufficient to support typical vector operations in a tiny soft-core;
- 52 • we present a complete yet very simple library of intrinsic functions to support  
53 application development, and we discuss the full detail of source code exploiting the co-  
54 processor instructions in each VGG-16 layer execution;
- 55 • we give insights into the open-source Klessydra processor core microarchitecture.

56 The rest of this article is organized as follows: Section 2 covers the related works on hardware  
57 acceleration for embedded computing on the IoT edge, including configurable solutions, Section 3  
58 introduces the Klessydra T1 processor soft-core featuring configurable hardware acceleration  
59 subsystem. Section 4 describes the fundamental features of the VGG-16 application case and its  
60 implementation on Klessydra T1. Section 5 reports and discusses the results obtained for the different  
61 sub-parts of the chosen application cases, and Section 6 summarizes the outcomes of the work.

## 62 2. Related works

63 Several previous works reported the design of hardware accelerated microcontroller cores  
64 implemented in edge-computing silicon chips. In [6], a RISC-V processor with DSP hardware support  
65 is presented, targeting near-threshold voltage operation. The Diet-SODA design implements a similar  
66 approach by running its DSP accelerator in near-threshold regime [7]. In [8,9,10,11] application  
67 specific accelerators are reported, based on highly parallel operation and minimized off-chip data  
68 movements for energy efficiency.

69 All of the above works focus on silicon implementation of units tailored to specific  
70 computations. As opposed to this view, the proposed hardware architecture study is independent of  
71 technology assumptions, such as the supply voltage, and addresses any physical implementation,  
72 particularly soft-cores on commercial FPGA devices, in the view of exploiting application-driven  
73 configurability. Regarding FPGA-based implementations, in [12] the authors present a cluster of  
74 RISC-V cores connected to a tightly-coupled scratchpad memory and a special purpose engine  
75 dedicated to convolutions only. Thanks to FPGA implementation, the convolution engine can be  
76 configured at synthesis time to optimize the execution of each convolutional layers, yet exhibiting a  
77 severe performance degradation when executing layers it was not built to optimize.

78 A recently published work [13] presents a SIMD configurable CNN coprocessor connected to a  
79 32-bit RV32IM RISC-V processor. Compared to the pure SIMD Klessydra configuration, that uses  
80 11678 LUTs and takes 824 clock cycles for a 4x4 matrix convolution, the work in [13] reports 12872  
81 LUTs and 2070 clock cycles.

82 In [14] the authors present a coprocessor soft-core at the edge of IoT, designed to be energy  
83 efficient in executing CNN as well as other machine learning algorithms. In particular, they explore  
84 the potential impact of data parallelism on the energy efficiency due the increased memory  
85 bandwidth. In our study, memory traffic as well as the memory static power consumption are taken  
86 into account in energy estimations.

87 The works in [15][16] present a pipelined CNN coprocessor capable of accelerating convolutions  
88 based on the extremely high parallelism in the coprocessor, yet limited to convolutional computation  
89 kernels.

90 In [17] the authors present different coprocessor configurations integrated with a parallel cluster  
91 of RISC-V cores and evaluated which of the configurations is the fastest and most energy efficient.  
92 They introduce special co-processing cores dedicated to the standard instruction subset RV32M,  
93 without exploring more sophisticated co-processor operations.

94 In [18] the authors provide a DCNN accelerator for IoT. The accelerator itself is designed to work  
95 with 3x3 kernels, and being not configurable, in order to support larger kernels they use a technique  
96 called kernel decomposition, which in fact increases the waste in computational resources and  
97 decreases in the energy efficiency, similarly to the convolution engine in [12].

98 The coprocessor architecture proposed in this work is general purpose in nature, being based on  
99 vector operations, and can be tailored to support a given computation kernel in the most efficient  
100 way. Our work builds on the preliminary developments reported in [2,4] and complements the  
101 analysis presented in [23].

102 The standard “V” vector extension of RISC-V – supported for example by SiFive products [24]  
103 and by the EPAC accelerator within the European Processor Initiative project [22]– is a large and  
104 complex instruction set extension, to cover applications ranging from embedded systems to HPC,  
105 which goes far beyond the scope of the lightweight Klessydra soft-core vector extension. Also, the  
106 standard “V” extension adopts a vector processing scheme based on a Vector Register File, while we  
107 explicitly chose to use generic Scratchpad Memories (SPMs) as local storage for more flexibility, at  
108 the price of losing compliance with any standard ISA extension. Rather than identifying vectors with  
109 a vector number chosen among 32 vector registers, we use pointers within the SPM address space to  
110 address vectors or portions of vectors. Also, as the number of SPMs available to the programmer in  
111 the microarchitecture is configurable.

112 The Ara processor [25], as well as the Xuantie-910 processor [26] and the dual core presented in  
113 [27], are all silicon ASIC implementations (thus not configurable as a soft-core is) of micro-  
114 architectures, which are actually not compliant with the “V” standard extension, yet they are still  
115 based on fixed Vector Register Files. Also, the Xuantie-910 processor addresses high performance  
116 superscalar execution of general-purpose non-vectorizable code, which is out of the scope of the  
117 Klessydra architecture.

118 The processor reported in [29] adopts an interesting approach based on directly converting ARM  
119 SVE vectorized code into a non-standard vector RISC-V extension, thus it is explicitly based on the  
120 same operation and storage scheme of ARM SVE. Klessydra diverges from this approach, favoring a  
121 broader exploration through configurability. The processor presented in [28] is a soft-core as  
122 Klessydra is, but it is again based on a Vector Register File rather than on a configurable SPM-based  
123 acceleration.

### 124 3. The Klessydra T1 customizable architecture

#### 125 *Hardware microarchitecture*

126 Klessydra is a family of open-source, RISC-V compliant and PULPino [20] compatible cores,  
127 which includes basic processors (T0 sub-family), hardware accelerated processors (T1 sub-family),  
128 and fault-tolerant processors (F0 sub-family) [21]. A characteristic feature of all Klessydra cores is the  
129 hardware support for interleaved multi-threading on a single core [1].  
130

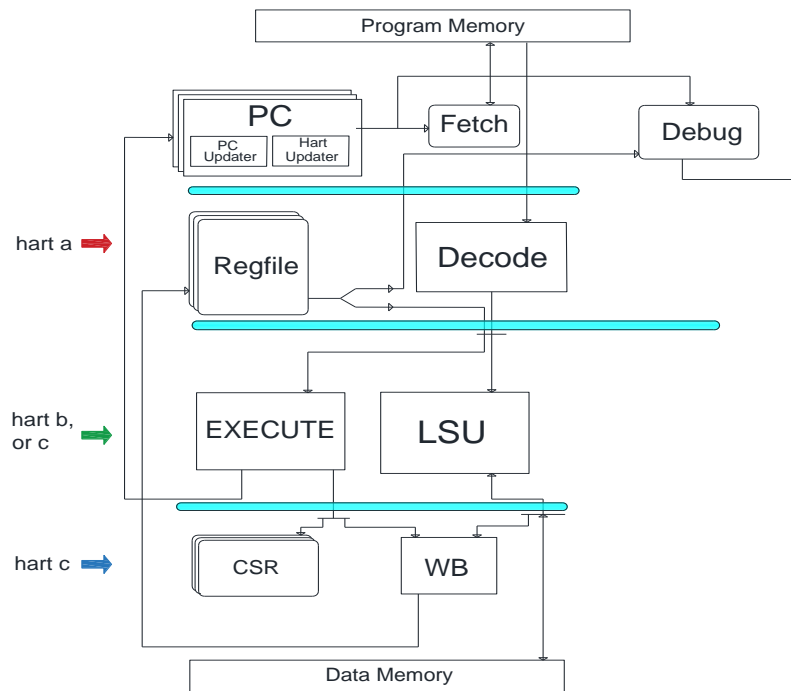


**Figure 1.** Klessydra T0 core microarchitecture

131  
 132  
 133  
 134  
 135  
 136  
 137  
 138  
 139  
 140  
 141  
 142  
 143  
 144  
 145  
 146  
 147  
 148  
 149  
 150  
 151

The hardware accelerated T1 cores are an extension of the basic T0 core, that is sketched in Figure 1. The T0 microarchitecture resembles a classic four-stage RISC pipeline, except for having multiple Program Counters to support multi-threading, and replicated register files and Control/Status Registers. Differently from a multi-core implementation, an interleaved multi-threading single core shares all the combinational logic constituting the instruction processing pipeline among the hardware threads (“harts” [3]), by interleaving threads in time, while maintaining separate PCs and registers to keep the state of each thread.

In each clock cycle a different Program Counter is used for instruction fetching, on a rotation basis. As a result, instructions belonging to different threads of execution are interleaved in the core pipeline, so that it is never possible that any two instructions in the pipeline manifest any register, structural or branch dependency. By fetching an instruction from a new thread in each clock cycle, pipeline hazards are eliminated, while if the same thread run for several clock cycles, its own data hazard or branching hazard would impose introducing dependency-check logic and pipeline stalling. The only dependency in the instruction pipeline can occur between two threads on explicit shared memory access, which is responsibility of the programmer.

The supported number of interleaved threads is a parameter of the synthesizable RTL code of the core.

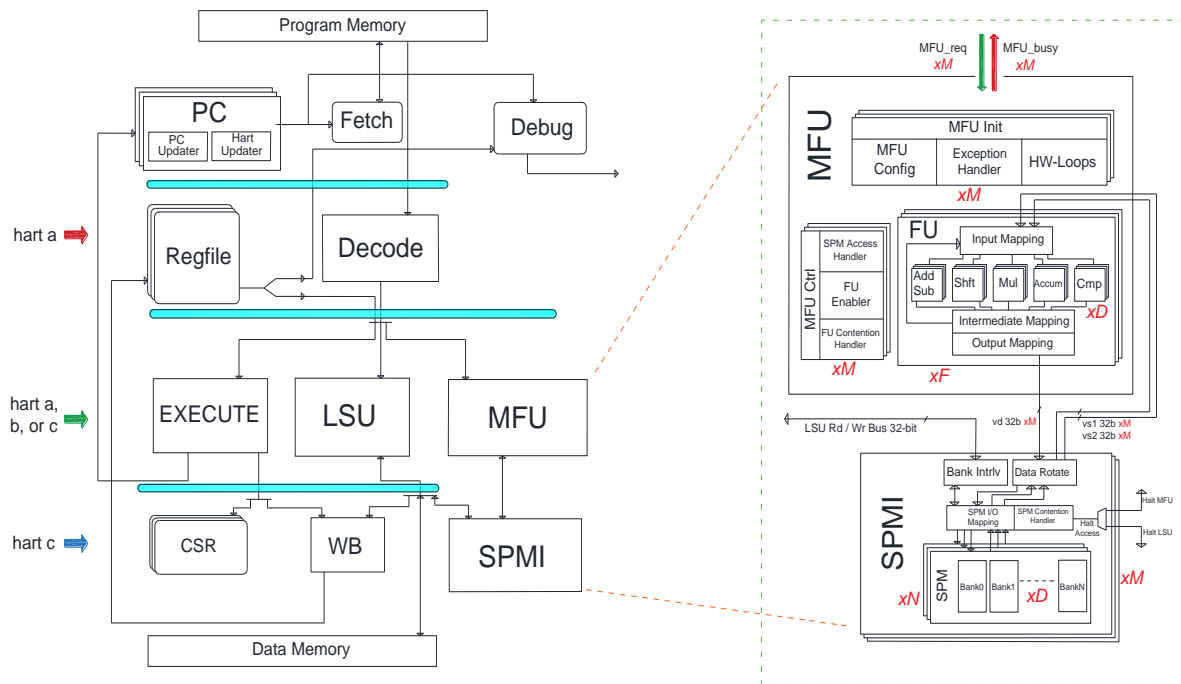


Figure 2. Klessydra T1 core microarchitecture

The T1 microarchitecture (Figure 2) is derived from the T0 by adding two execution units, namely the Load-Store Unit (LSU) and the Vector Co-processing Unit (VCU), the latter being internally comprised of Multi-Purpose Functional Units (MFU) and Scratch-Pad Memory Interface (SPMI).

At the instruction level, the T1 architecture supports the parallel execution of instructions of different types, belonging to the same hart. In fact, the LSU works in parallel with the other units when executing memory store instructions, that cannot cause a write-back conflict on the register file. The MFU is allowed to read operands from the register file but can only write its results to local scratchpad memories (SPMs), thus keeping the SPMs and the Registerfile decoupled and allowing parallel execution between instructions writing to each of these memories simultaneously. Scalar instructions of a hart are processed by the “Execution” unit and operate on data in the Register File, while vector instructions are processed by the VCU and operate on data in the SPMs. Data transfers to/from the data memory from/to the SPMs are managed by the LSU via dedicated instructions.

The MFUs execute vector arithmetic instructions, whose latency is proportional to the vector length. In an in-order interleaved-multi-threading pipeline, a hart requesting access to the busy MFUs may result in stalling the whole pipeline, stalling other harts that may not need to access the MFU. To circumvent this, in the T1 architecture, the waiting hart executes a self-referencing jump so that the PC for that hart does not advance until the MFU becomes free, avoiding unnecessary stalls of harts that are independent from the MFU being busy. Figure 3 demonstrates a cycle accurate diagram of the mechanism.

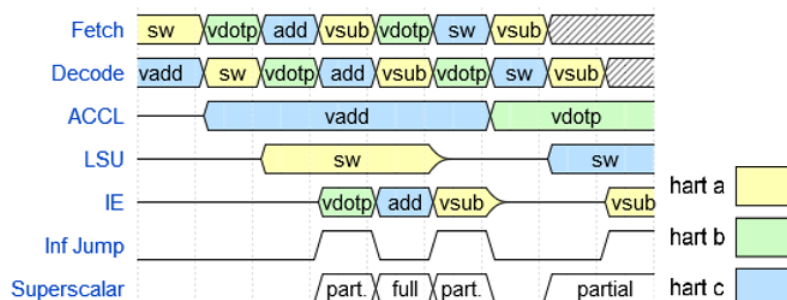


Figure 3. Hart interleaving and hart stall timing diagram

152  
153  
154  
155  
156  
157  
158  
159  
160  
161  
162  
163  
164  
165  
166  
167  
168  
169  
170  
171  
172  
173  
174  
175

176  
177

178

179

180

181

182

183

184

185

186

187

188

189

190

191

192

193

194

195

196

197

198

199

200

201

202

When deploying Klessydra T1 in a IoT edge device, one can configure the number of parallel lanes  $D$  in the MFU, the number of MFUs  $F$ , the SPM capacity, the number of independently accessible SPMs  $N$  in each SPMI, the number of SPMs  $M$ , as well as the way the MFUs and SPMI are shared between the harts. Representative configurations are the following:

- **Thread-Shared coprocessor:** All harts in the core share a single MFU/SPM subsystem. Harts in this scheme are required to execute an infinite jump when trying to access the MFU when its busy. In this approach, instruction level parallelism is limited to occur only between coprocessor instructions writing to the SPM and non-coprocessor instructions writing to the main memory or register file. To mitigate the delays on a hart executing an infinite jump, the coprocessor here may exploit pure data level parallelism (DLP) acceleration, by SIMD execution.
- **Thread-Dedicated coprocessor:** Each hart is appointed a full MFU/SPM subsystem, eliminating inter-hart coprocessor contention and allowing inter-coprocessor parallel execution. Stalls can only happen if the next instruction of the same hart that is using the MFU requests an MFU operation. DLP by SIMD execution can still be exploited in this approach, but also thread level parallelism (TLP) by fully symmetric MIMD execution, allowing execution of multiple vector instructions in parallel, .
- **Thread-Dedicated SPMs with a Shared MFU:** The harts here maintain a dedicated SPM address space, yet they share the functional units in the MFU. This scheme still allows inter-hart parallel execution of coprocessor instructions, provided they use different internal functional units of the MFU (e.g, adder, multiplier). Harts that request a busy internal unit in the MFU will be stalled, and their access will be serialized until the contended unit becomes free, while harts that request a free functional unit can work in parallel with the other active harts in the MFU. DLP by SIMD execution can still be exploited in this approach, but also TLP by heterogeneous MIMD execution.

203

204

Table 1 summarizes the design parameters and corresponding configurations, whose names will be used as references in reporting performance results.

**Table 1.** Summary of explored hardware configurations.

<b>M</b> (number of SPMI units)	<b>F</b> (Number of FMUs)	<b>D</b> (number of lanes in FMU)	<b>Execution paradigm</b>
1	1	1	SISD
1	1	2, 4, 8	Pure SIMD
3	3	1	Symmetric MIMD
3	3	2, 4, 8	Symmetric MIMD + SIMD
3	1	1	Heterogenous MIMD
3	1	2, 4, 8	Heterogenous MIMD + SIMD

205

206

#### Programming paradigm

207

208

209

210

211

By default, a Klessydra core runs the maximum number of hardware threads (which is a synthesis parameter) allowed by the microarchitecture. The function `Klessydra_get_coreID()` can read the id number of the thread executing the function from the MHARTID CSR register, so this allows to distinguish threads and possibly have each thread to execute a different piece of program. Figure 4 shows a generic C program skeleton in which each of three threads executes its own instruction

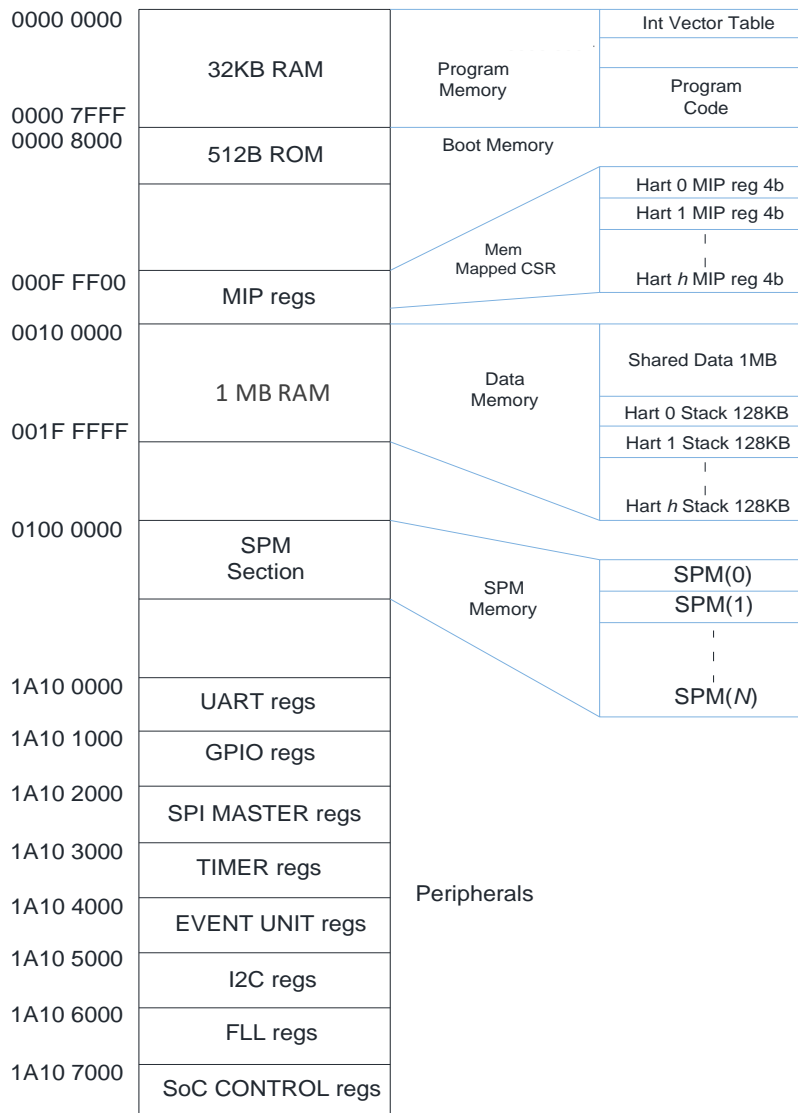
212 flow. The functions *sync\_barrier\_thread\_registration()* and *sync\_barrier()* allow implementing a  
 213 synchronization barrier by based on inter-thread software interrupts, to synchronize thread  
 214 execution at certain points of the program.  
 215

```

sync_barrier_thread_registration(); //Executed by all threads
if (Klessydra_get_coreID()==0){
    // thread_0 subroutine
}
if (Klessydra_get_coreID()==1){
    // thread_1 subroutine
}
if (Klessydra_get_coreID()==2){
    // thread_2 subroutine
}
sync_barrier(); //Executed by all threads
    
```

216  
 217  
 218  
 219

**Figure 4.** Code for multi-threaded execution on Klessydra-T1



220  
 221  
 222

**Figure 5** Klessydra T1 memory map.

223 Figure 5 gives a representation of the memory map assumed by the Klessydra T1 operation.

224 The SPM local storage is visible to the programmer as a specific address region in the memory  
 225 map. The programmer can move data to/from any point of the SPM address space with no constraint  
 226 except the total capacity of the SPMs, which in turn is a parameter of the microarchitecture design.

227 Inter-thread data transfers may happen via shared global static variables allocated in the main  
 228 data memory or, in the case of a shared coprocessor configuration, via shared SPM address space. As  
 229 in any multi-threading execution scheme, access to shared data must be accompanied by explicit  
 230 thread synchronization, which is available in Klessydra by means of specific intrinsic functions  
 231 implementing semaphore locks compliant with RISC-V atomic instructions, not in the scope of this  
 232 work.

233 The custom instruction extension supported by the VCU and LSU is summarized in Table 2. The  
 234 instructions supported by the coprocessor sub-system are exposed to the programmer in the form of  
 235 very simple intrinsic functions, fully integrated in the RISC-V gcc compiler toolchain. The compiler  
 236 does not have knowledge of the hardware configuration, so it only translates the intrinsic functions  
 237 into the corresponding dedicated vector instructions, which are then executed by the hardware  
 238 according to the chosen hardware configuration. The instructions implement vector operations  
 239 working on the memory space mapped on the local SPMs. The vector length applied by MFU  
 240 operations is encoded in a user accessible custom control/status register (CSR) named MVSIZE.

**Table 1.** RISC-V instruction set custom extension for Klessydra-T processors

<i>Assembly syntax – (r) denotes memory addressing via register r</i>	<i>Function declaration</i>	<i>Short description</i>
<code>kmemld (rd), (rs1), (rs2)</code>	<code>kmemld( void* rd, (void*) rs1, (int) rs2);</code>	<i>load vector into scratchpad region</i>
<code>kmemstr (rd), (rs1), (rs2)</code>	<code>kmemstr( void* rd, (void*) rs1, (int) rs2);</code>	<i>store vector into main memory</i>
<code>kaddv (rd), (rs1), (rs2)</code>	<code>kaddv( void* rd, (void*) rs1, (void*) rs2);</code>	<i>adds vectors in scratchpad region</i>
<code>ksubv (rd), (rs1), (rs2)</code>	<code>ksubv( void* rd, (void*) rs1, (void*) rs2);</code>	<i>subtract vectors in scratchpad region</i>
<code>kvmul (rd), (rs1), (rs2)</code>	<code>kvmul( void* rd, (void*) rs1, (void*) rs2);</code>	<i>multiply vectors in scratchpad region</i>
<code>kvred (rd), (rs1)</code>	<code>kvred( void* rd, (void*) rs1);</code>	<i>reduce vector by addition</i>
<code>kdotp (rd), (rs1), (rs2)</code>	<code>kdotp( void* rd, (void*) rs1, (void*) rs2);</code>	<i>vector dot product into register</i>
<code>ksvaddsc (rd), (rs1), (rs2)</code>	<code>ksvaddsc( void* rd, (void*) rs1, (void*) rs2);</code>	<i>add vector + scalar into scratchpad</i>
<code>ksvaddrf (rd), (rs1), rs2</code>	<code>ksvaddrf( void* rd, (void*) rs1, (int) rs2);</code>	<i>add vector + scalar into register</i>
<code>ksvmulsc (rd), (rs1), (rs2)</code>	<code>ksvmulsc( void* rd, (void*) rs1, (void*) rs2);</code>	<i>multiply vector + scalar into scratchpad</i>
<code>ksvmulrf (rd), (rs1), rs2</code>	<code>ksvmulrf( void* rd, (void*) rs1, (int) rs2);</code>	<i>multiply vector + scalar into register</i>
<code>kdotpps (rd), (rs1), (rs2)</code>	<code>kdotpps( void* rd, (void*) rs1, (void*) rs2);</code>	<i>vector dot product and post scaling</i>
<code>ksrlv (rd), (rs1), rs2</code>	<code>ksrlv( void* rd, (void*) rs1, (int) rs2);</code>	<i>vector logic shift within scratchpad</i>
<code>ksrav (rd), (rs1), rs2</code>	<code>ksrav( void* rd, (void*) rs1, (int) rs2);</code>	<i>vector arithmetic shift within scratchpad</i>
<code>krelu (rd), (rs1)</code>	<code>krelu( void* rd, (void*) rs1);</code>	<i>vector ReLu within scratchpad</i>
<code>kvslt (rd), (rs1), (rs2)</code>	<code>kvslt( void* rd, (void*) rs1, (void*) rs2);</code>	<i>compare vectors and create mask vector</i>
<code>ksvslt (rd), (rs1), rs2</code>	<code>ksvslt( void* rd, (void*) rs1, (int) rs2);</code>	<i>compare vector-scalar and create mask</i>
<code>kvcp (rd), (rs1)</code>	<code>ksrlv( void* rd, (void*) rs1);</code>	<i>copy vector within scratchpad region</i>
<code>csr MVSIZE, rs1</code>	<code>mvsize( int rs1 );</code>	<i>vector length setting</i>
<code>csr MVTYPE, rs1</code>	<code>mvttype( int rs1 );</code>	<i>element width setting (8,16,32 bits)</i>
<code>csr MPSCLFAC, rs1</code>	<code>mpscfac( int rs1 );</code>	<i>post scaling factor (kdotpps instruction)</i>



242

243 **4. VGG-16 implementation on Klessydra T1**244 *Implementation workflow*

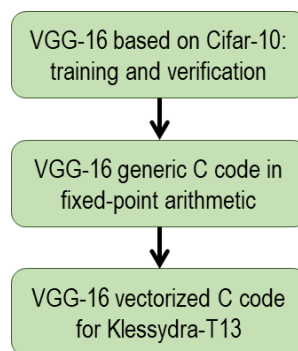
245 VGG-16 is a deep Convolutional Neural Network (CNN) used in computer vision for  
246 classification and detection tasks, consisting of 13 convolutional layers, 5 maxpooling layers, 2 fully-  
247 connected layers and one output/softmax layer. The original VGG-16 can label a 224x224 pixel RGB  
248 image to one class out of 1000, using approximately 554MB space for 32-bit floating-point weights  
249 and bias values.

250

251

252

253



254

**Figure 6.** Workflow for the VGG-16 implementation

255

256

257 In the view of a realistic IoT edge embedded scenario, we implemented a VGG-16 derivation  
258 based on the widely known CIFAR-10 dataset, targeting 10 classes and 32x32 pixel RGB images and  
259 requiring 135 MB for weights and bias values. Table 3 reports the breakdown of the inference  
260 algorithm layers constituting the Cifar-10 VGG-16. The layers 19 to 21 do not compute operations on  
261 matrices, rather they implement dot-product operations between vectors of different sizes, similarly,  
layer 22 implements a Softmax function on a vector of length 10.

262

**Table 2.** Cifar-10 VGG-16 inference layers

Layer number	Computation type	Matrix size
1	<i>Convolution</i>	32x32
2	<i>Convolution</i>	32x32
3	<i>Max Pool</i>	16x16
4	<i>Convolution</i>	16x16
5	<i>Convolution</i>	16x16
6	<i>Max Pool</i>	8x8
7	<i>Convolution</i>	8x8
8	<i>Convolution</i>	8x8
9	<i>Convolution</i>	8x8
10	<i>Max Pool</i>	4x4
11	<i>Convolution</i>	4x4
12	<i>Convolution</i>	4x4
13	<i>Convolution</i>	4x4
14	<i>Max Pool</i>	2x2
15	<i>Convolution</i>	2x2
16	<i>Convolution</i>	2x2
17	<i>Convolution</i>	2x2
18	<i>Max Pool</i>	1x1
19	<i>Fully connected</i>	512x512
20	<i>Fully connected</i>	4096x4096
21	<i>Fully connected</i>	4096x4096
22	<i>Softmax</i>	10

263

264

265

266

267

268

269

270

271

272

273

274

275

276

277

278

Figure 6 illustrates the workflow to implement a Cifar-10 VGG-16 application on the Klessydra processor platform. Notably, since the target hardware platform supports fixed-point arithmetic, we based the implementation on fixed-point weights and data. We set the integer part to 11 bits and the fractional part to 21 bits, which leads an accuracy drop from 98.04% to 84.01% on the of output results of the inference. We remark that re-training the network, as well as further algorithmic optimizations, such as quantization and compression techniques, are not in the scope of the present work. The verification phase of the network in fixed point arithmetic was done via Matlab Deep Learning Toolbox. In order to be able to exploit the C language intrinsic functions of the Klessydra platform, the original Matlab code for VGG-16 was ported to C code. This generic C code implementation was used as the basis for the subsequent vectorization to exploit the hardware co-processor, and it was also used to run the same algorithm on the reference platforms used for performance comparison. We verified that no additional loss of quality is introduced by the proposed hardware architecture, which produces an identical output to the C fixed-point version executed on a general purpose computer.

279

*Generic fixed-point C code porting*

280

281

The generic C code used for convolutional layers is reported in Figure 7. Image convolutions are implemented using the zero-padding technique: the feature map (FM) matrix is converted into a new

282 matrix having two additional rows and columns of zeros on its borders, to avoid having filter  
 283 elements without corresponding pixel values when the centroid element of the 3x3 kernel slides along  
 284 the borders. As a general feature of the implementation, multiplications always need a pre-scaling  
 285 and post-scaling operation in order to re-align the fixed-point representation of the result. The  
 286 *convolution2D()* function performs the pre-scaling when creating the zero-padded matrix and also  
 287 pre-scales the kernel values. The convolution is carried out by nested for loops, by which the Kernel  
 288 map (KM) matrix slides across the input image with a stride of one element. The partial result of each  
 289 multiplication is pre-scaled and added to the corresponding output pixel, completing the multiply  
 290 and accumulate step. After the convolution is complete, a bias value is added to the output feature  
 291 map, and the ReLU non-linear activation function is executed across all the matrix elements to  
 292 conclude the convolutional layer.

```

a) for (int i = 0; i < layer_outputs; i++){ //scan for every output matrix
    output_pt = &output_fm[i][0][0];
    for (int k = 0; k < layer_inputs ; k++){ //scan for every input matrix
        for (int w=0; w<9; w++) kern.kernel_9[w]=layer_filters[(output_pt*9)+w];
        convolution2D(MATRIX_SIZE, input_fm[k], kern.kernel_9, output_pt);
    } //convolutions are completed
    bias = layer_bias[i];
    addBias(MATRIX_SIZE, output_pt, bias);
    relu(MATRIX_SIZE, output_pt);
} //the output matrix is complete

b) for (i = 1; i < (size+2)-1; i++){
    for (j = 1; j < (size+2)-1; j++){
        output_pixel[(i-1)*size+(j-1)]
            += ( FM_zeropad[i-1][j-1] * kernel[0] ) >> post_scale ;
    } //end of loop for first kernel element
    //...
    for (j = 1; j < (size+2)-1; j++){
        output_pixel[(i-1)*size+(j-1)]
            += ( FM_zeropad[i+1][j+1] * kernel[8] ) >> post_scale ;
    } //end of loop for last kernel element
} //end of loop "i"

c) //Adding the Bias value
for (int i = 0; i < size; i++)
    for (int j = 0; j < size; j++)
        matrix[j + size*i] += bias;
//ReLU function
for (int i = 0; i < size; i++)
    for (int j = 0; j < size; j++)
        if (input[j + size*i] < 0) {
            input[j + size*i] = 0;
        } else continue;
  
```

293  
 294 **Figure 7.** (a) Convolutional layer in generic C code; (b) Convolution2D function inner operations; (c)  
 295 Bias addition and ReLU function inner operations (Layers: 1,2,4,5,7,8,9,11,12,13,15,16,17)

296  
 297 Figure 8 reports the C code adopted for Maxpool layers. The Maxpool layer halves the width and  
 298 height of the FMs, sliding across them a 2x2 window, with a stride equal to two, filtering all the values  
 299 except for the highest of the batch. In this way the most important features detected from the image  
 300 are passed at the successive layers.  
 301

```

a) for (k = 0; k < layer_outputs; k++) {
    input_pt = &input_fm[k][0][0];
    output_pt = &output_fm[k][0][0];
    maxpool(input_size, input_pt,
            output_size, output_pt);
}

b) for (int m = 0; m < size_i; m+=2){
    for (int n = 0; n < size_i; n+=2){
        max = FM[n + size_i*m];
        for (i = m; i < m+2; i++){
            for (j = n; j < n+2; j++){
                if (FM[j + size_i*i] > max)
                    max = FM[j + size_i*i];
            }
        }
        output[index++] = max;
    }
}

```

302  
303  
304  
305

**Figure 8.** (a) Maxpool layer in generic C code; (b) Maxpool function inner operations (Layers: 3,6,10,14,18)

```

a) pt_layer_filters = &fully_connect_filter_array[0];
    pt_layer_bias = &fully_connect_fibias_array[0];
    input_pt = &input_vector[0];
    for (i = 0; i < layer_outputs_elements; i++) {
        getWeights(pt_layer_filters, number_of_elements, buffer);
        output_vector[i] = fullyconnect(number_of_elements, input_pt, buffer);
        bias = getBias(pt_layer_bias);
        output_vector[i] += bias;
    } //the output vector is complete

b) for(int i=0; i<dim ; i++){
    tmp1=vect_1[i]>>pre_scale;
    tmp2=vect_2[i]>>pre_scale;
    output += (tmp1*tmp2)>>post_scale;
}
return output;

c) for (int i = 0; i < vector_lenght; i++){
    sum = sum + exp(output[i]);
}
for (int i = 0; i < vector_lenght; i++){
    output[i] = exp(output[i])/SUM ;
}

```

306

307

**Figure 9.** (a) Fully-connected layer in generic C code; (b) Fully-connect inner operations; (c) Softmax layer inner operations (Fully-connected Layer: 19,20,21; Softmax Layer: 22)

308

309

310

311

312

313

314

315

316

317

### Vectorized C code implementation

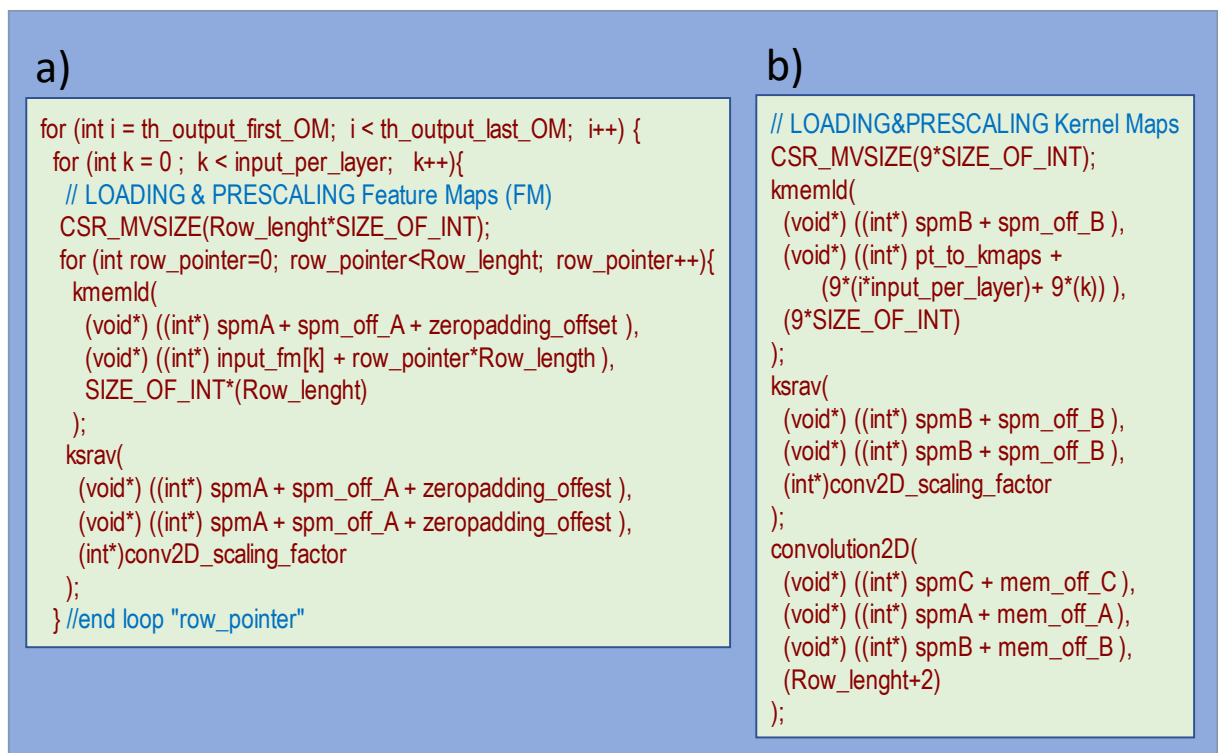
318

319

320

Program code vectorization targeting the Klessydra intrinsic function library is based on two types of intervention: data movement to efficiently exploit the scratchpad memory sub-system, and vector arithmetic operation exploiting the accelerator functional unit.

321 A loop of *kmemld()* functions transfer the FM and KMs operands into two SPMs, that we refer to  
 322 as *spmA* and *spmB*, from the main memory. To implement zero-padding, when loading the feature  
 323 maps into *spmA*, we first reset the SPM content to zero and then proceed with loading bursts of data  
 324 from the FM rows, with exact offsets that grant the correctness of zero-padding. Figure 10(a) displays  
 325 the code executed to set up the FM in *spmA*. The offsets added to the pointers passed to the *Kmemld()*  
 326 function allow for the implementation zero-padding. The *ksrav()* function implements fixed-point  
 327 pre-scaling by performing an arithmetic right shift operation of a vector. It requires a pointer to the  
 328 vector, a pointer to store the resulting vector and a shift amount. Figure 10(b) similarly shows the  
 329 loading and pre-scaling of the 9-element KM into *spmB* and also the calling sequence of the  
 330 *convolution2D()* function.  
 331  
 332



333  
 334 **Figure 10.** (a) Zero-padded, pre-scaled FM setup in SPM; (b) Pre-scaled KM collection in SPM and  
 335 calling sequence of *convolution2D()* (Layers: 1,2,4,5,7,8,9,11,12,13,15,16,17)  
 336

337 The *Convolution2D()* function requires the addresses of the FM and KM first elements in *spmA*  
 338 and *spmB*, an address pointing to a region in *spmD* for temporary value storage, and the address to  
 339 store the output matrix in *spmC*. Figure 11 reports the internal operations, which are built upon  
 340 knowing which vectors are to be multiplied as the kernel map slides across all the input map pixels.  
 341 Taking into account which elements will be multiplied when the kernel completely slides across a  
 342 row of the FM, and the fact that this process is replicated for every row, we can multiply the FM row  
 343 values with the corresponding scalar from the KM, and update the output matrix (OM) row with a  
 344 vector of partial results. This process is straightforward and allows to fully exploit the vector  
 345 coprocessor capabilities by using matrix rows as vector operands.  
 346

```

CSR_MVSIZE(Row_size);
for(i=Zeropad_off; i Row_size-Zeropad_off; i++){
  k_element=0;
  for(FM_row_pointer=-Zeropad_off; FM_row_pointer <= Zeropad_off; FM_row_pointer++){
    for (column_offset=0; column_offset < kernel_size; column_offset++){
      FM_offset= (i+FM_row_pointer)*Row_size+column_offset;
      ksvmulsc(SPM_D, (SPM_A+FM_offset), (SPM_B + k_element++));
      ksraV(SPM_D, SPM_D, scaling_factor);
      OM_offset = (Row_size*i)+Zeropad_off;
      kaddv((SPM_C+OM_offset),(SPM_C+OM_offset),SPM_D);
    }
  }
}

```

347

348

349

350

351

352

353

354

355

356

357

358

359

360

361

**Figure 11.** Convolution2D inner loops operations (Layers: 1,2,4,5,7,8,9,11,12,13,15,16,17)

Referring to Figure 11, after setting the vector length, the loop with index “i” scans the rows of the output matrix (OM); the *FM\_row\_pointer* loop and the *column\_offset* loop iterate three times each to cover the necessary vector-scalar product required for the 3x3 kernel matrix. The *FM\_offset* variable points to the proper FM row in *spmA*, from which the source vector is fetched. The *ksvmulsc()* function performs the scalar-vector multiplication between an FM row vector and a KM scalar, and the result is post-scaled by the *ksrav()* function for fixed-point alignment. The *kaddv()* function performs the vector addition, updating the OM row in *spmC*.

After the convolutions are done, the OM is updated with the addition of the bias value (Figure 12(a)). A *kmemld()* is required to have the single scalar value in the scratchpad memory, then the whole matrix is updated by *ksvaddsc\_v2()*, which performs the vector plus scalar operation and includes a fourth parameter to adjust the vector length prior to doing the calculation.

a)	b)
<pre> //Preload the spm_B with the bias value kmemld(   (void*)((int*)spmB + mem_off_B),   (void*)(pt_to_bs+offset),   (SIZE_OF_INT) ); //update the whole matrix with the bias ksvaddsc_v2(   (void*) ((int*) spmC + mem_off_C),   (void*) ((int*) spmC + mem_off_C),   (void*) ((int*) spmB + mem_off_B),   ((Row_lenght+2)*(Row_lenght+2)     *SIZE_OF_INT) ); </pre>	<pre> krelu(   (void*)( (int*)spmC + mem_off_C ),   (void*)( (int*)spmC + mem_off_C ) ); //perform the ReLU on the output matrix for (int row_pt=0; row_pt&lt;run_SIZE; row_pt++){   kmemstr(     (void*)&amp;output_fm[i][0][0] + (row_pt*run_SIZE) ,     (void*)((int*)spmC + mem_off_C +       ((row_pt+1)*(run_SIZE+2)+1) ),     SIZE_OF_INT*(run_SIZE)   ); } //end kmemstr loop for retrieving of the OM in main memory kbcst((void*)((int*)spmC + mem_off_C), (void*)zero_value ); </pre>

362

363

364

365

366

367

368

**Figure 12.** (a) Adding the bias to the Output Matrix; (b) Applying the ReLU function to the Output Matrix (Layers: 1,2,4,5,7,8,9,11,12,13,15,16,17)

As the last part of the convolutional layers, the ReLU non-linear function is applied to all the OM pixels, which is stored back in main memory. The SPM region is cleared for the next iteration of the loop by broadcasting a zero value into the target memory region with *kbcst()* (Figure 12(b)).

369 The maxpooling layer is executed on the OM in main memory, through conventional scalar  
 370 instructions, following the same implementation of the generic C code.

371 The fully-connected layer is comprised of a computation kernel based on dot products (Figure  
 372 13(a)). The source vector is moved into spmA as a single burst of data using the *kmemld()*  
 373 and pre-scaled by *ksrav()*. A loop handles the properly transposed loading of the neurons parameters  
 374 into spmB. The two vectors in the SPMs are processed by the dot-product function *kdotpps()*, which  
 375 includes a post-scaling of the product before accumulation for fixed point alignment.

376 After the end of the loop, the vector of bias values is moved into spmD then added to the output  
 377 vector of the layer. The result vector is processed by the *krelu()* function, and then it is stored back to  
 378 the main memory. The *kbcast()* function clears the spmC memory space (Figure 13(b)).

379 The softmax layer is executed in main memory through conventional scalar instructions, with  
 380 the same implementation of the generic C code.

```

a) kmemld( (void*)spmA, (void*)((int*)pt_to_vector), vector_lenght*SIZE_OF_INT);
   CSR_MVSIZE(vector_lenght*SIZE_OF_INT);
   ksrav( (void*)spmA, (void*)spmA, scaling factor);
   for (int loop_index = 0; loop_index < divisor_0; loop_index++){
       kmemld(
           (void*)((int*)spmB + mem_off_B),
           (void*)((int*)pt_to_wh + (loop_index*vector_lenght)),
           (vector_lenght*SIZE_OF_INT));
       CSR_MVSIZE(vector_lenght*SIZE_OF_INT);
       ksrav( (void*)((int*)spmB + mem_off_B), (void*)((int*)spmB + mem_off_B), scaling factor);
       kdotpps( (void*)spmC + loop_index, (void*)((int*)spmA), (void*)((int*)spmB + mem_off_B
           ));
   }

b) kmemld( (void*)spmD, (void*)(pt_to_bs), (vector_lenght*SIZE_OF_INT) );
   kaddv( (void*)spmC, (void*)spmC, (void*)spmD );
   punt_out = &layer_output[0];
   krelu( (void*)spmC, (void*)spmC );
   kmemstr( (void*)punt_out, (void*)spmC, (vector_lenght*SIZE_OF_INT) );
   kbcast( (void*)spmC, (void*)zero );
  
```

381

382 **Figure 13.** Fully-connected layer operations. (a) Dot-product kernel; (b) Bias addition and ReLu (Fully-  
 383 connected Layer: 19,20,21).

384

385 The exact execution of the vectorized VGG-16 inference program running on Klessydra T1 cores  
 386 was verified by comparing the full output produced by RTL simulation against the general purpose  
 387 VGG-16 fixed-point C code running on an X86 server.

388

## 389 5. Performance and Power analysis

### 390 Setup

391 All Klessydra cores are compatible with the PULPino processor platform [20]. Yet, the  
 392 original PULPino memory subsystem cannot support the execution of the full VGG-16  
 393 inference algorithm, which requires 255 MB storage for the constant data consisting of the  
 394 neural network weights, and at least 1 MB memory space for global and local variables. Thus,  
 395 we extended the PULPino memory sub-system to include 256 MB of addressable physical



396 data memory, partitioned into a 1 cycle latency 1 MB RAM to be mapped on the FPGA  
 397 BRAM, and a 6 cycle latency 255MB space mapped on an external flash memory device,  
 398 connected via SPI interface. The 1 MB RAM is the physical mapping of the portion of the  
 399 data memory address space that is dedicated to dynamically allocated data.

400 The program memory is 32 KB mapped in the FPGA BRAM.

401 The modified PULPino platform featuring Klessydra T1 processor cores was synthesized on  
 402 a Kintex7 FPGA board using the Vivado tool flow. The design entry was the RTL  
 403 VHDL/SystemVerilog description of the platforms under analysis. The C code of the  
 404 VGG16 application was compiled by the RISC-V gcc tool chain to produce the binary code  
 405 chain to produce the binary code executable by the target processors. The execution of the  
 406 application on the target processors was simulated both as RTL and post-synthesis gate level,  
 407 to verify the correct functionality and to extract the signal activity for power estimation in  
 408 Vivado. Table 4 reports the hardware resource utilization and the maximum clock frequency  
 409 producing zero or positive slack, for all the processor configurations under analysis.  
 410

**Table 3.** Area and frequency summary of the Klessydra-T cores equipped with to 1MB Data Mem.

Configuration	Hardware Utilization					Top Freq. [MHz]
	FF	LUT	DSP	B-RAM	LUT-RAM	
SISD (M=1,F=1,D=1)	2482	7083	11	88	264	132.1
Pure SIMD (M=1,F=1,D=2)	2664	9010	15	88	264	127.0
Pure SIMD (M=1,F=1,D=4)	3510	11678	23	88	264	125.5
Pure SIMD (M=1,F=1,D=8)	4904	18531	39	88	264	112.6
Symmetric MIMD (M=3,F=3,D=1)	3509	10701	19	120	264	114.2
Symmetric MIMD+SIMD (M=3,F=3,D=2)	4659	16556	31	120	264	113.9
Symmetric MIMD+SIMD (M=3,F=3,D=4)	6746	27485	55	120	264	108.9
Symmetric MIMD+SIMD (M=3,F=3,D=8)	11253	52930	103	120	264	96.3
Heterogenous MIMD (M=3,F=1,D=1)	3025	10655	11	120	264	119.9
Heterogenous MIMD+SIMD (M=3,F=1,D=2)	3741	17161	15	120	264	115.7
Heterogenous MIMD+SIMD (M=3,F=1,D=4)	4767	25535	23	120	264	110.4
Heterogenous MIMD+SIMD (M=3,F=1,D=8)	7303	48066	39	120	264	91.5
No accl	1409	4079	7	72	176	194.6
RI5CY	1307	6351	6	72	0	65.1
Zeroriscy	1605	2834	1	72	0	77.2

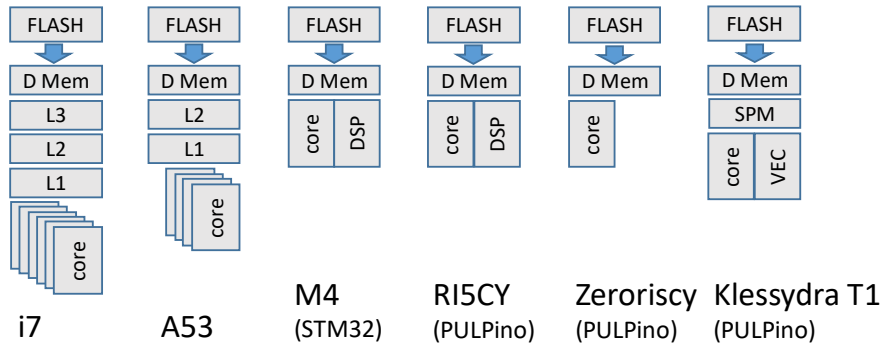
411  
 412 The VGG-16 inference fixed-point code was also implemented on the following alternative  
 413 computing systems, to accomplish a comprehensive comparative analysis:

- 414 • An FPGA board featuring a soft-processor comprised of the extended PULPino platform  
 415 equipped with the DSP-accelerated RI5CY core, reaching 65 MHz clock frequency;
- 416 • An FPGA board featuring a soft-processor comprised of the extended PULPino platform  
 417 equipped with a Zeroriscy core [19], reaching 77 MHz clock frequency;
- 418 • An STM32 single board computer featuring an 84 MHz ARM Cortex M4 core with DSP  
 419 extension, 96 KB data memory;



420  
421  
422  
423  
424

- A Raspberry-PI 3b+ single board computer featuring a 1.4 GHz ARM Cortex A53 quad-core CPU, 16 KB L1 cache and 512 KB L2 cache, 1 GB LPDDR2 main memory;
- An x86 single board computer featuring a 3 GHz exa-core, 12-thread i7 CPU, 384 KB L1 cache, 1.5 MB L2 cache, 9 MB LLC, 8 GB DDR4 main memory.



425  
426

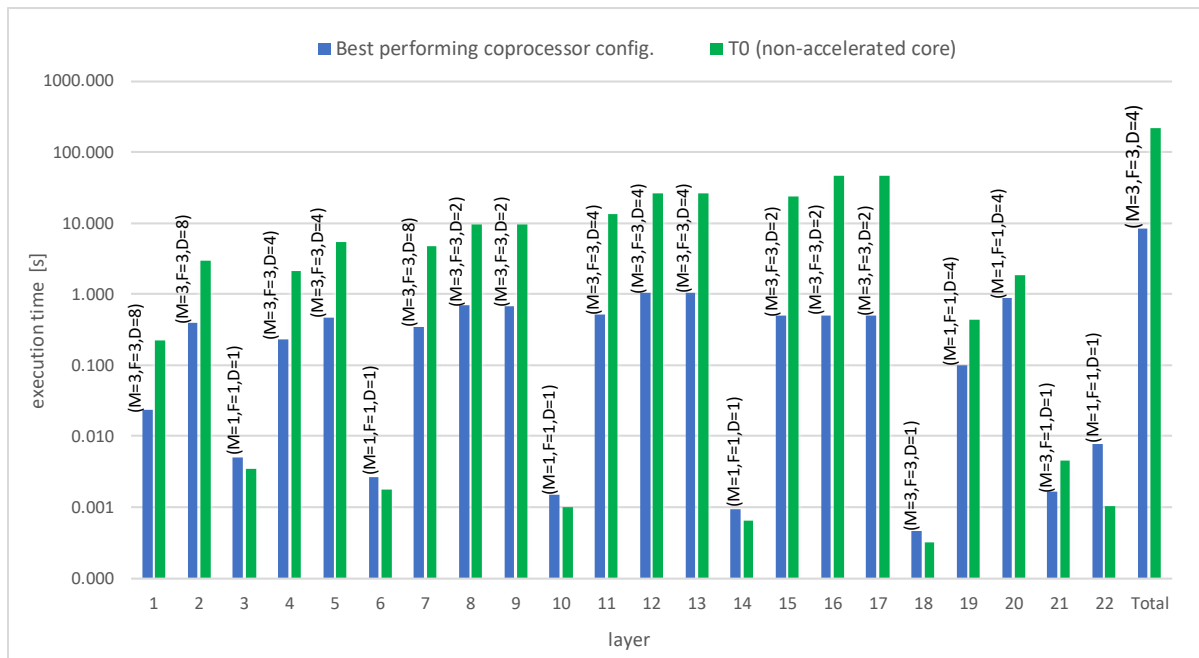
**Figure 14.** System architecture organization of the compared boards

427

428 The system architecture organization corresponding to the devices under comparison are sketched  
429 in Figure 14. The read-only storage space dedicated to the VGG-16 weights is hosted by an SPI-  
430 connected Flash memory expansion board in all the considered architectures, and the weights are  
431 preemptively loaded into the main RAM space for the inference algorithm execution.

432 *Results*

433 The first phase of performance analysis targeted the detailed account of the performance of each  
434 coprocessor hardware microarchitecture.

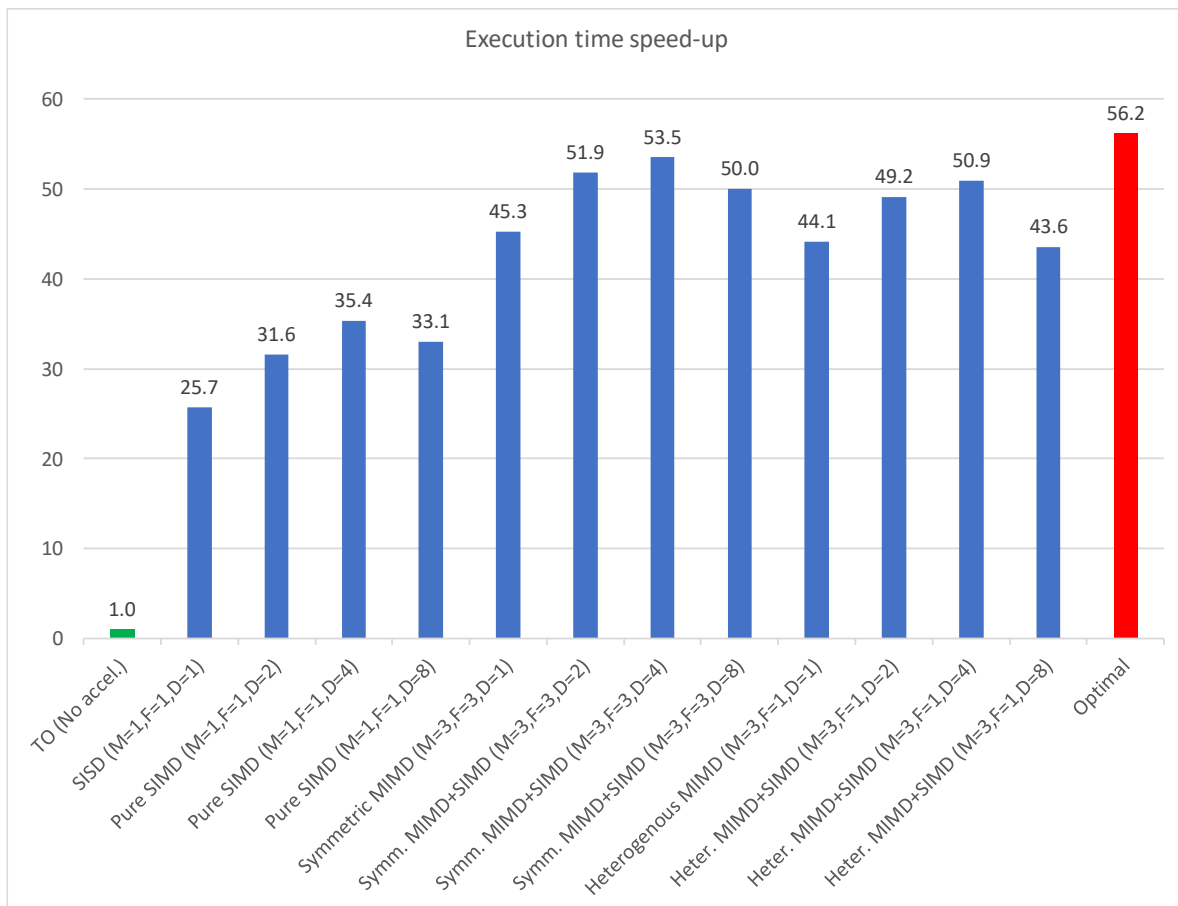


435  
436  
437  
438  
439

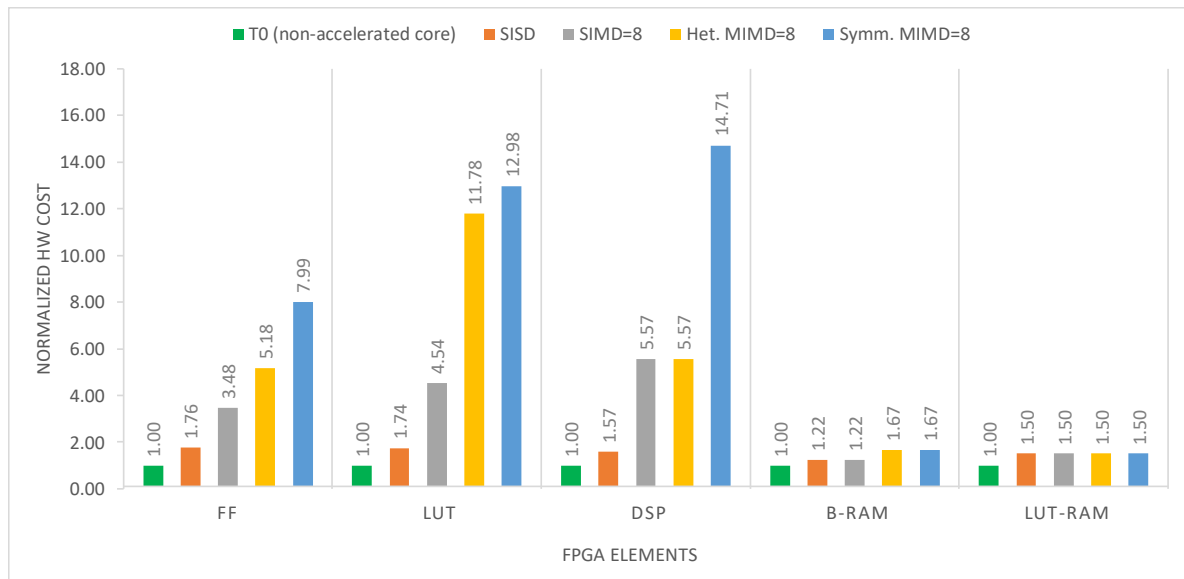
**Figure 15** Absolute execution time [s] of the best performing accelerated configuration and of the non-accelerated T0 core, per layer.

440 Figure 15 shows the execution time obtained by the best performing of all the explored T1  
441 coprocessor configurations and by the non-accelerated T0 core, for each VGG-16 layer. The results  
442 give evidence to the fact that the performance of the coprocessor hardware configurations varies with  
443 the algorithm layer it executes. The Symmetrical MIMD configurations with D ranging between 2

444 and 8 result to be the best performing for the convolutional layers, while the pure SIMD  
 445 configurations with  $D = 4$  results to be the optimal choice for the largest Fully Connected layers.  
 446 Notably, the Maxpool and Softmax layers exhibit worse execution time in the accelerated cores than  
 447 with in the non-accelerated T0 core, because in the present software implementation they are  
 448 executed as scalar computation, and so the data transfer to/from the SPMs constitutes an overhead  
 449 with no corresponding vector computation acceleration. Nonetheless, the relative impact of those  
 450 layers on the overall execution time is negligible, as shown by the logarithmic scale.  
 451 Figure 16 presents the total VGG16 inference execution time speed-up obtained by each coprocessor  
 452 configuration over the non-accelerated T0 core. The diagram also includes the ideal speed-up  
 453 obtained assuming to use the optimal configuration for each layer. Figure 17 represents the hardware  
 454 cost of the configurations that exhibit the highest speed-up, normalized to the non-accelerated T0  
 455 core hardware cost, for a direct comparison. The resulting hardware utilization efficiency is notable,  
 456 as the maximum speed-up is over 50X, while the maximum hardware cost overhead is well below  
 457 15X.  
 458  
 459



460  
 461 **Figure 16.** Total execution time speed-up over non-accelerated core obtained by each coprocessor  
 462 configuration, along with the speed-up obtained by using the optimal configuration for each layer  
 463  
 464  
 465  
 466  
 467



468

469

**Figure 17** Hardware overhead normalized to the non-accelerated T0 core.

470

471

472

473

474

475

476

477

478

Figure 18 shows the total energy consumed by the most efficient of all the explored T1 coprocessor configurations and by the non-accelerated T0 core, for each VGG-16 layer. Again, the optimal coprocessor configuration for energy efficiency depends on the layer being executed. Optimal energy efficiency, unlike absolute performance, swings between Pure SIMD and Symmetrical MIMD configurations. Similarly to the execution time analysis, for pure scalar computation layers the energy consumption worsens in the vector-accelerated microarchitecture, due to the SPM data transfer overhead. Yet, the overall impact of those layers on the total energy is negligible as shown by the logarithmic scale.

479

480

481

482

483

484

Figure 19 gives significance of the total energy saving obtained by each coprocessor configuration over the non-accelerated T0 core. The energy saving is expressed as the fraction of the energy consumed in the accelerated core over the energy consumed in the non-accelerated core, obtaining energy consumption between 6.4% and 4% of the non-accelerated core (energy saving between 93.6% and 96%). The diagram also includes the ideal energy reduction obtained assuming to use the optimal configuration for each layer.

485

486

487

488

489

490

Figure 16 and Figure 19 evidence the ideal performance limit achievable by dynamically changing the coprocessor microarchitecture at no overhead, via software controlled Dynamic Partial Reconfiguration (DPR) of the FPGA, so that the system always uses the optimal hardware scheme for speed or energy efficiency according to the computation kernel being executed. The storage, power and time overhead associated to DPR is not included in the analysis, and should be the subject of specific experiments.

491

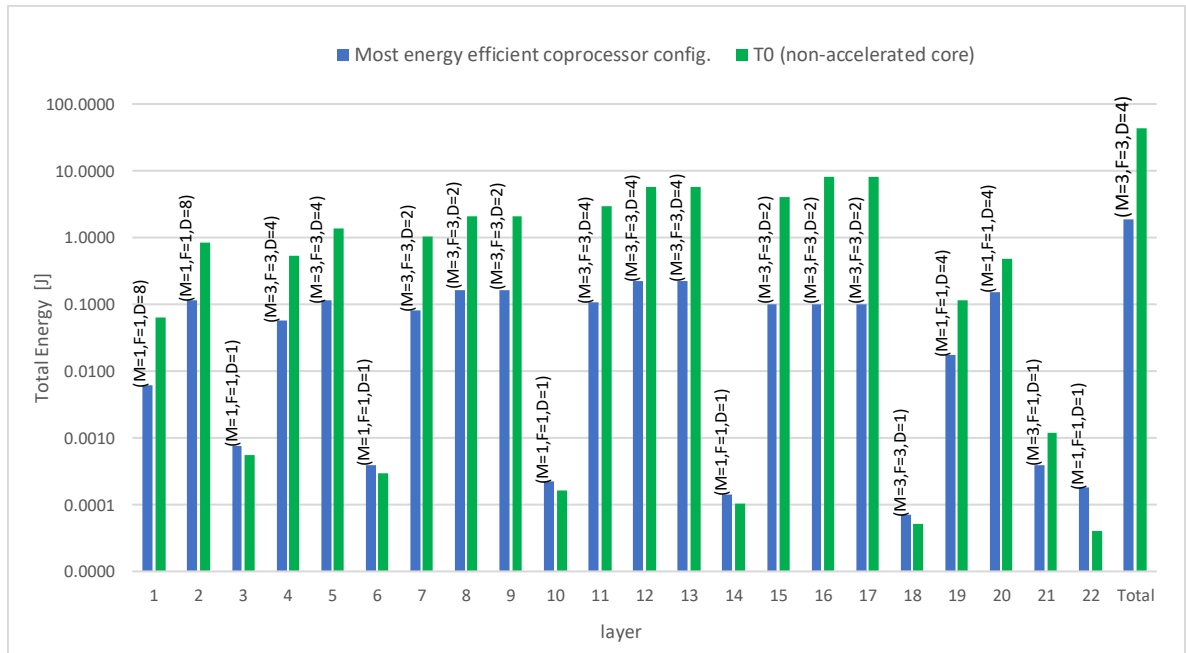
492

493

494

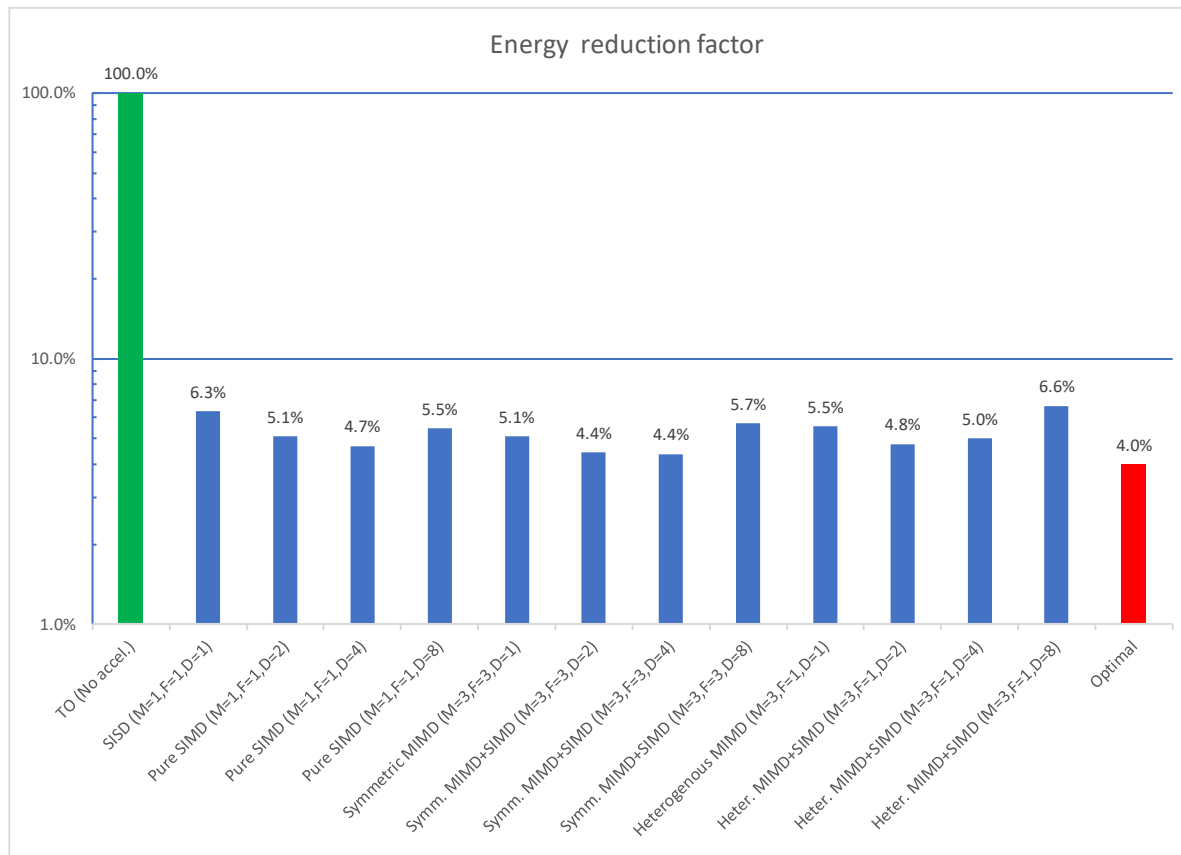
495

The second phase of performance analysis aimed at comparing the efficiency of the proposed soft-processor architecture with the alternative hardware architecture solutions for the execution of the same application. In this analysis, the proposed solution consisted of the extended PULPino platform equipped with the Klessydra T1 core + optimal vector coprocessor for each layer being executed.



496  
497  
498  
499  
500  
501

**Figure 18** Total energy consumption [J] of the most energy efficient coprocessor configuration and of the non-accelerated T0 core, per layer



502  
503  
504  
505

**Figure 19.** Energy reduction factor with respect to non-accelerated core (lower is better) obtained by each coprocessor configuration, along with the energy obtained by using the optimal configuration for each layer

506 Table 5 summarizes the performance comparison results, expressed as total execution time, total  
 507 energy consumption, and average energy consumed per algorithmic operation. Algorithmic  
 508 operations are the data multiplications and additions that are inherent to the algorithm being  
 509 computed, and do not depend on the actual software implementation. The absolute execution time  
 510 obviously favors high-end computing devices, yet the results give evidence of the effectiveness of the  
 511 Klessydra T1 customizable vector coprocessor sub-system with respect to other single-core PULPino  
 512 soft-processor FPGA implementations. Also, the energy efficiency results show the potential  
 513 advantage of a Klessydra T1 vector-accelerated soft-processor FPGA implementation, with respect to  
 514 general purpose single-board computers.

**Table 5.** Performance comparison with alternative solutions

Processor	Time [s]	Energy [J]	Energy per op [pJ/op]
Core i7 PC board	0.08	2.90	21
Cortex A53 Raspberry Pi 3	0.89	2.32	17
Cortex M4 STM32	117.78	7.77	55
RI5CY PULPino on FPGA	444.30	40.06	285
Zeroriscy PULPino on FPGA	548.04	38.90	277
Klessydra-T1 PULPino on FPGA	7.91	1.74	12

515

## 516 6. Conclusion

517 The validation of the VGG-16 inference output data produced by Klessydra processors against  
 518 conventional processors demonstrated how the Klessydra open-source infrastructure can be used for  
 519 implementing configurable RISC-V soft-cores equipped with hardware acceleration for vector  
 520 computing on FPGA. The detailed porting of the target application routines has been documented in  
 521 this work. Performance results show the effectiveness of the Klessydra microarchitecture scheme,  
 522 built upon interleaved multi-threading and vector coprocessor hardware acceleration, with respect  
 523 to other FPGA-based single-core solutions. Looking at energy efficiency, the Klessydra FPGA soft-  
 524 core solution shows superior performance with respect to commercial single-board computers that  
 525 may be used as IoT extreme-edge devices.

526 The results of the performance analysis conducted on the Klessydra T1 vector coprocessor  
 527 schemes demonstrate the dependency of the optimal hardware configuration on the algorithm layer  
 528 being executed. This evidence opens the way to the development of software configurable  
 529 accelerators and further to the implementation of self-adapting coprocessor microarchitectures in IoT  
 530 extreme-edge nodes.

531 **Supplementary Materials:** The Klessydra processor core family and accelerators are openly available online at  
 532 <https://www.github.com/klessydra>

## 533 References

- 534 1. Cheikh, A., Cerutti, G., Mastrandrea, A., Menichelli, F. and Olivieri, M., 2017, September. The  
 535 microarchitecture of a multi-threaded RISC-V compliant processing core family for IoT end-nodes. In  
 536 International Conference on Applications in Electronics Pervading Industry, Environment and  
 537 Society(pp. 89-97). Springer, Cham.
- 538 2. Olivieri, M., Cheikh, A., Cerutti, G., Mastrandrea, A., and Menichelli, F., "Investigation on the optimal  
 539 pipeline organization in RISC-V multi-threaded soft processor cores", In 2017 New Generation of CAS  
 540 (NGCAS), pp. 45-48. IEEE, 2017.
- 541 3. RISC-V Instruction Set specifications. [Online] "<https://riscv.org/specifications/>"

- 542 4. Cheikh, A., Sordillo, S., Mastrandrea, A., Menichelli, F. and Olivieri, M., 2019, September. Efficient  
543 Mathematical Accelerator Design Coupled with an Interleaved Multi-threading RISC-V  
544 Microprocessor. In International Conference on Applications in Electronics Pervading Industry,  
545 Environment and Society (pp. 529-539). Springer, Cham.
- 546 5. Samie, F.; Bauer, L.; Henkel, J. "From Cloud Down to Things: An Overview of Machine Learning in  
547 Internet of Things". IEEE Internet Things J. 2019, 4662, 1.
- 548 6. Gautschi, M., Schiavone, P., Traber, A., Loi, I., Pullini, A., Rossi, D., Flamand, E., Gürkaynak, F.,  
549 Benini, L., "Near-threshold RISC-V core with DSP extensions for scalable IoT endpoint devices." IEEE  
550 Trans. on Very Large Scale Integration (VLSI) Systems 25, no. 10 (2017): 2700-2713.
- 551 7. Seo, S., Dreslinski, R.G., Woh, M., Chakrabarti, C., Mahlke, S. and Mudge, T., 2010, August. Diet SODA:  
552 A power-efficient processor for digital cameras. In Proceedings of the 16th ACM/IEEE international  
553 symposium on Low power electronics and design (pp. 79-84).
- 554 8. Chen, Y.H., Krishna, T., Emer, J.S. and Sze, V., 2016. Eyeriss: An energy-efficient reconfigurable  
555 accelerator for deep convolutional neural networks. IEEE journal of solid-state circuits, 52(1), pp.127-  
556 138.
- 557 9. Moini, S., Alizadeh, B., Emad, M. and Ebrahimpour, R., 2017. A resource-limited hardware accelerator  
558 for convolutional neural networks in embedded vision applications. IEEE Transactions on Circuits and  
559 Systems II: Express Briefs, 64(10), pp.1217-1221.
- 560 10. Du, L., Du, Y., Li, Y., Su, J., Kuan, Y.C., Liu, C.C. and Chang, M.C.F., 2017. A reconfigurable streaming  
561 deep convolutional neural network accelerator for Internet of Things. IEEE Transactions on Circuits  
562 and Systems I: Regular Papers, 65(1), pp.198-208.
- 563 11. Conti, Francesco, and Luca Benini. "A ultra-low-energy convolution engine for fast brain-inspired  
564 vision in multicore clusters." In 2015 Design, Automation & Test in Europe Conference & Exhibition  
565 (DATE), pp. 683-688. IEEE, 2015.
- 566 12. Meloni, P., Deriu, G., Conti, F., Loi, I., Raffo, L. and Benini, L., 2016, May. Curbing the roofline: a  
567 scalable and flexible architecture for CNNs on FPGA. In Proceedings of the ACM International  
568 Conference on Computing Frontiers (pp. 376-383).
- 569 13. Wu, N., Jiang, T., Zhang, L., Zhou, F. and Ge, F., 2020. A Reconfigurable Convolutional Neural  
570 Network-Accelerated Coprocessor Based on RISC-V Instruction Set. Electronics, 9(6), p.1005.
- 571 14. Watanabe, D., Yano, Y., Izumi, S., Kawaguchi, H., Takeuchi, K., Hiramoto, T., Iwai, S., Murakata, M.  
572 and Yoshimoto, M., 2020. An Architectural Study for Inference Coprocessor Core at the Edge in IoT  
573 Sensing. In 2020 2nd IEEE International Conference on Artificial Intelligence Circuits and Systems  
574 (AICAS) (pp. 305-309). IEEE.
- 575 15. Wu, Y., Wang, J.J., Qian, K., Liu, Y., Guo, R., Hu, S.G., Yu, Q., Chen, T.P., Liu, Y. and Rong, L., 2020.  
576 An energy-efficient deep convolutional neural networks coprocessor for multi-object detection.  
577 Microelectronics Journal, p.104737.
- 578 16. Chang, M.C., Pan, Z.G. and Chen, J.L., 2017, October. Hardware accelerator for boosting convolution  
579 computation in image classification applications. In 2017 IEEE 6th Global Conference on Consumer  
580 Electronics (GCCE) (pp. 1-2). IEEE.
- 581 17. Lima, P., Vieira, C., Reis, J., Almeida, A., Silveira, J., Goerl, R. and Marcon, C., 2020, March. Optimizing  
582 RISC-V ISA Usage by Sharing Coprocessors on MPSoC. In 2020 IEEE Latin-American Test Symposium  
583 (LATS) (pp. 1-5). IEEE.
- 584 18. Du, L., Du, Y., Li, Y., Su, J., Kuan, Y.C., Liu, C.C. and Chang, M.C.F., 2017. A reconfigurable streaming  
585 deep convolutional neural network accelerator for Internet of Things. IEEE Transactions on Circuits  
586 and Systems I: Regular Papers, 65(1), pp.198-208.
- 587 19. Schiavone P.D., Conti F., Rossi D., Gautschi M., Pullini A., Flamand E., Benini L., Slow and steady wins  
588 the race? a comparison of ultra-low-power risc-v cores for internet-of-things applications. In 2017 27th  
589 International Symposium on Power and Timing Modeling, Optimization and Simulation (PATMOS)  
590 2017 Sep 25 (pp. 1-8). IEEE.
- 591 20. Traber A, Gautschi M., PULPino: datasheet. ETH Zurich, University of Bologna. 2017 Jun 9.
- 592 21. Blasi L, Vigli F, Cheikh A, Mastrandrea A, Menichelli F, Olivieri M. A RISC-V Fault-Tolerant  
593 Microcontroller Core Architecture Based on a Hardware Thread Full/Partial Protection and a Thread-  
594 Controlled Watch-Dog Timer. In International Conference on Applications in Electronics Pervading  
595 Industry, Environment and Society 2019 Sep 11 (pp. 505-511). Springer, Cham.

- 596 22. European Processor Initiative (EPI), EU H2020 research and innovation programme GA No 826647,  
597 [Online] "<https://www.european-processor-initiative.eu/project/epi/>".
- 598 23. A. Cheikh, S. Sordillo, A. Mastrandrea, F. Menichelli, G. Scotti and M. Olivieri, "Klessydra-T: Designing  
599 Vector Coprocessors for Multi-Threaded Edge-Computing Cores," in IEEE Micro, doi:  
600 10.1109/MM.2021.3050962.
- 601 24. Online: <https://www.sifive.com/blog/risc-v-vector-extension-intrinsic-support>
- 602 25. M. Cavalcante, F. Schuiki, F. Zaruba, M. Schaffner and L. Benini, "Ara: A 1-GHz+ Scalable and Energy-  
603 Efficient RISC-V Vector Processor With Multiprecision Floating-Point Support in 22-nm FD-SOI," in  
604 *IEEE Transactions on Very Large Scale Integration (VLSI) Systems*, vol. 28, no. 2, pp. 530-543, Feb. 2020
- 605 26. C. Chen *et al.*, "Xuantie-910: A Commercial Multi-Core 12-Stage Pipeline Out-of-Order 64-bit High  
606 Performance RISC-V Processor with Vector Extension : Industrial Product," *2020 ACM/IEEE 47th*  
607 *Annual International Symposium on Computer Architecture (ISCA)*, Valencia, Spain, 2020, pp. 52-64
- 608 27. J. C. Wright *et al.*, "A Dual-Core RISC-V Vector Processor With On-Chip Fine-Grain Power  
609 Management in 28-nm FD-SOI," in *IEEE Transactions on Very Large Scale Integration (VLSI) Systems*, vol.  
610 28, no. 12, pp. 2721-2725, Dec. 2020
- 611 28. M. Johns and T. J. Kazmierski, "A Minimal RISC-V Vector Processor for Embedded Systems," *2020*  
612 *Forum for Specification and Design Languages (FDL)*, Kiel, Germany, 2020
- 613 29. Y. Kimura, T. Kikuchi, K. Ootsu and T. Yokota, "Proposal of Scalable Vector Extension for Embedded  
614 RISC-V Soft-Core Processor," *2019 Seventh International Symposium on Computing and Networking*  
615 *Workshops (CANDARW)*, Nagasaki, Japan, 2019, pp. 435-439
- 616



© 2021 by the authors. Submitted for possible open access publication under the terms and conditions of the Creative Commons Attribution (CC BY) license (<http://creativecommons.org/licenses/by/4.0/>).